Grid Resolution Study of Ground Water Flow and Transport

by Kathleen M. Bower[1], Carl W. Gable[2], and George A. Zyvoloski[3]

Abstract

Three-dimensional grids representing a heterogeneous, ground water system are generated at 10 different resolutions in support of a site-scale flow and transport modeling effort. These grids represent hydrostratigraphy near Yucca Mountain, Nevada, consisting of 18 stratigraphic units with contrasting fluid flow and transport properties. The grid generation method allows the stratigraphy to be modeled by numerical grids of different resolution so that comparison studies can be performed to test for grid quality and determine the resolution required to resolve geologic structure and physical processes such as fluid flow and solute transport. The process of generating numerical grids with appropriate property distributions from geologic conceptual models is automated, thus making the entire process easy to implement with fewer user-induced errors. The series of grids of various resolutions are used to assess the level at which increasing resolution no longer influences the flow and solute transport results. Grid resolution is found to be a critical issue for ground water flow and solute transport. The resolution required in a particular instance is a function of the feature size of the model, the intrinsic properties of materials, the specific physics of the problem, and boundary conditions. The asymptotic nature of results related to flow and transport indicate that for a hydrologic model of the heterogeneous hydrostratigraphy under Yucca Mountain, a horizontal grid spacing of 600 m and vertical grid spacing of 40 m resolve the hydrostratigraphic model with sufficient precision to accurately model the hypothetical flow and solute transport to within 5% of the value that would be obtained with much higher resolution.

Introduction

The ground water hydrology and possible radionuclide transport pathways from the potential underground high-level nuclear waste repository located near Yucca Mountain, Nevada, are currently being evaluated. The Yucca Mountain Project uses geologic and hydrologic information gathered from many sources (Czarnecki et al. 1997). This information is used to model ground water flow and potential radionuclide transport (Civilian Radioactive Waste Management System Management and Operating Contractor 2000; Luckey et al. 1996; Eddebbarh et al. 2003; Zyvoloski et al. 2003). The construction of computational grids to reflect geologic structure and stratigraphy for flow

[1]Geology/Geography Department, Eastern Illinois University, 600 Lincoln Ave., Charleston, IL 61920-3099; cfkmb1@eiu.edu

[2]Corresponding author: Earth and Environmental Sciences, MS T003, Los Alamos National Laboratory, Los Alamos, NM 87545; gable@lanl.gov

[3]Earth and Environmental Sciences, MS T003, Los Alamos National Laboratory, Los Alamos, NM 87545; gaz@lanl.gov

and transport numerical models can be a formidable task. The quality of these grids with respect to numerical truncation error and accuracy of representation of hydrogeology is of foremost importance to the Yucca Mountain Project. In fact, an understanding of the quality of the grids is necessary to having a defensible model. One of the challenges facing a researcher in a project of this magnitude is understanding the tradeoff between a high-resolution model that represents hydrostratigraphy with a high degree of fidelity and a lower resolution model that is more suited to making the large number of calculations necessary for repository safety or performance assessment evaluation. The errors resulting from using a model with too low of a resolution for heterogeneous aquifers are described in detail by Haitjema et al. (2001). The modeling challenge can be met in various ways including accepting some amount of error, using the telescopic mesh refinement approach (Ward et al. 1987), or using large computational resources. For example, Frind et al. (1988) use a dual scale (local vs. aquifer) approach to solve for the large-scale flow field, as well as the local dispersive processes. In a study of the Macrodispersion Experiment site on the Columbus Air Force Base in Mississippi (Feehley et al. 2000), statistical methods are

used to create hydraulic conductivity distributions, but still a dual-domain mass transfer approach was needed to match solute transport because small-scale flow pathways were not explicitly represented in the discretization. This work does not address issues of interpretation and interpolation of data for the construction of a three-dimensional geological model. The focus is on creating flow and transport model grids that capture the geometric detail of a particular geological model. This paper is motivated by challenges in modeling the ground water flow near Yucca Mountain.

The process of developing ground water flow models can be divided into three parts: (1) characterizing geology and developing conceptual models of the geology and hydrologic material properties, (2) building the grid and prescribing boundary and initial conditions, and (3) applying the computational physic models of fluid flow, energy transport, and chemical transport (Gable et al. 1996). Tools to integrate and automate this process (GEOMESH, X3D, LaGriT) (Gable et al. 1995; Trease et al. 1996; George 2000) are described and used in this project. Throughout the text, the term GEOMESH will refer to all three of these packages developed from similar origins.

Geologic interpretation, stratigraphic model development, and material characterization are performed based on numerous field measurements and are described in Czarnecki et al. (1997) and D'Agnese et al. (1997). The stratigraphic model, populated with hydrologic material properties, provides the basic framework for computational grid building. The ability of the computational grid to represent the geologic complexity directly affects the accuracy of the numerical model's approximation of the physical system. Grid generation can be tedious, time consuming, and prone to errors, especially for models representing complex structures such as faults and stratigraphy with pinch-outs and layer truncations. GEOMESH is a grid generator that uses the stratigraphic model developed in the characterization step to create a grid that represents complex structure and stratigraphy. Any physical or chemical attribute (e.g., permeability, porosity, rock type) can be traced numerically from field measurement to grid generation. Resulting grids are then inspected visually, as well as algorithmically checked with grid quality measures. The grids are then used to numerically model mass, energy, and chemical transport.

The automated processes that accomplish the three parts of geologic flow modeling make the entire process easier to execute with fewer errors. At any step in the process, it is relatively straightforward to incorporate greater grid resolution in a particular subregion or to define new boundary conditions or new material attributes. This set of computer tools is allowing very complicated geologic volumes to be accurately and efficiently modeled. By facilitating model modification, numerical modeling can be done in which geometry and grid resolution are part of the suite of parameters that are varied to provide insight into the sensitivity of results to changes.

Quality control issues involved cannot be overemphasized. We believe that a system that uses only algorithmic processing of the hydrogeologic data is necessary because the steps can be quantified and metrics of goodness of representation can be established. These metrics include a volume comparison between the stratigraphic model hydrogeologic units and the computational model hydrogeologic units. The metrics could also include measures of grid element quality such as distributions of element volume, element aspect ratio, and finite volume nodal coefficients.

The hydrostratigraphy represented in the geologic model (Figure 1) of Yucca Mountain (Figure 2) consists of multiple layers of hydrostratigraphic units with contrasting fluid flow and transport properties. The hydrostratigraphy of the saturated zone at the site is characterized in some detail and has been described by D'Agnese et al. (1997) and Czarnecki et al. (1997) from surface and subsurface data. Figure 1 shows the geometric distribution of material types along various cross sections. An unstructured grid containing 2,557,063 tetrahedral elements with horizontal resolution of 250 m and variable vertical resolution defines this model of the hydrostratigraphy. We are interested in the effect of using a number of structured grids with different resolutions on the fluid flow and solute transport results for this hydrostratigraphy model. At what resolution is the geometry of the material distribution precisely represented in order to model the hypothetical fluid flow and potential solute transport through the aquifer? Since higher grid resolution is more expensive, the modeler can use this information to determine what the desired accuracy of flow simulations is and at what resolution of grids that accuracy would be attained.

Control Volume Finite Element Method

The control volume finite element (CVFE) method or finite volume (FV) method is used to perform the ground water modeling. FV methods are based upon the idea that a continuum may be modeled as a configuration of discrete elements. For each element, equations are written that describe the interaction of the element with its neighbors. These equations describe the hydrologic behavior of the elements. The method leads to a set of nonlinear equations that are then solved. For a detailed presentation of the finite volume method, refer to Forsyth (1989) and Forsyth (1991). The FEHM (finite element heat and mass) code is used to perform all ground water flow calculations. FEHM is a nonisothermal, multiphase flow and transport code. It simulates the flow of water and air and the transport of heat and solutes in two- and three-dimensional saturated or partially saturated heterogeneous porous media. The code includes comprehensive reactive geochemistry and transport modules, and a particle tracking capability. Fractured media can be simulated using an equivalent continuum, discrete fracture, dual porosity, or dual permeability approach. For a detailed description of FEHM, the control volume finite element code used for this work, refer to Zyvoloski et al. (1991).

Only the conservation of mass equations are shown, as the energy equations are not used for this study. The equations shown are for an isotropic, isothermal medium though these restrictions do not exist in FEHM. The conservation of fluid mass is

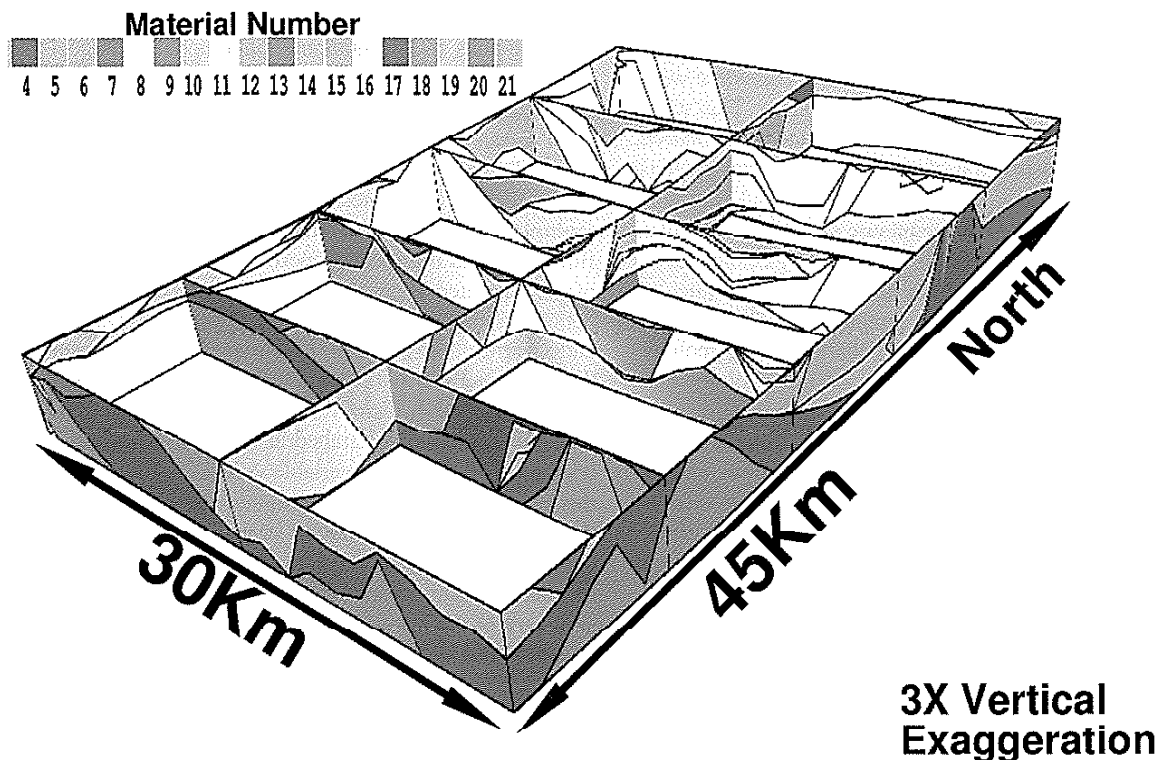$$\frac{\partial A_{mass}}{\partial t} + \nabla \cdot \vec{f}_{mass} + q_{mass} = 0$$

(1)

Figure 1. Cross sections of saturated zone geological model. Table 1 relates material number to geological unit names.

where A_{mass} (M/L^3) is the fluid mass per unit volume given by

$$A_{mass} = \phi\rho \tag{2}$$

$\vec{f}_{mass}$ (M/L^{3}t) is the fluid mass flux given by

$$\vec{f}_{mass} = \rho\vec{v} \tag{3}$$

ϕ is the porosity in the system, ρ (M/L^3) is the fluid density, $\vec{v}$ (L/t) is the fluid velocity, and q_{mass} (M/L^{3}t) is the fluid mass source. The velocity of the fluid is expressed by Darcy's law:

$$\vec{v} = -\frac{k}{\mu}\nabla(P - \rho\vec{g}) \tag{4}$$

where P (M/Lt^2) is fluid pressure, μ (M/Lt) is the dynamic viscosity of the fluid, k (L^2) is the permeability, and $\vec{g}$ (L/t^2) is the acceleration due to gravity. The calculations presented are for constant density water so we convert results to head rather than presenting the pressure solution. Using a reference density, $\rho = 1000$ (kg/m^3), $\vec{g} = 9.8$ (m/s^2), and elevation z, referenced to mean sea level, pressure is converted to head using, $h = z + P/(\rho g)$.

The conservation of solute equation is explicitly coupled to the fluid flow field. The conservation equation for a single component, nonreacting solute in a constant density fluid in a saturated media is

$$\frac{\partial A_s}{\partial t} = \nabla \cdot (\rho\phi D_s\nabla C_s) - \nabla \cdot \vec{f}_s - q_c \tag{5}$$

where $A_s = \phi C_s\rho$ is the solute mass storage per unit total volume for aqueous component liquid concentration, C_s (moles/M) is the concentration of the solute, D_s (L^2/t) is the dispersion coefficient, $\vec{f}_s = \rho C_s\vec{v}$ is the advective mass flux of solute, and q_c (moles/ L^{3}t) is the solute source or sink. For a complete description of these features, see Robinson et al. (1997) and Viswanathan et al. (1998).

A CVFE approach is used in FEHM. The CVFE method has been used extensively in petroleum reservoir engineering (Heinemann and Brand 1988; Forsyth 1989; Palagi and Aziz 1991; Verma 1996). A desirable feature of CVFE formulation is that it insures local mass conservation and upstream weighting (Verma 1996). Delaunay triangles (finite elements) in two dimensions and Delaunay tetrahedra in three dimensions are divided into volumes surrounding nodes. In this application, the nodal volumes are Voronoi polyhedra (Voronoi 1908; Okabe et al. 1992) associated with each node. Voronoi volumes are a specific type of control volume composed of convex polyhedra for which all space inside the polyhedra is closer to the enclosed node than to any other node (Figure 3). An explicit definition of a Voronoi tessellation is as follows. For a set of points $P = \{p_1, p_2,...p_n\}$ where $2 \leq n < \infty$ and $\overline{x}_j \neq \overline{x}_i$ for $i \neq j$, the Voronoi polygons in 2D or polyhedra in 3D are defined as the set of convex regions

$$V(p_i) = \{\overline{x} \mid \|\overline{x} - \overline{x}_i\| \leq \|\overline{x} - \overline{x}_j\| \text{ for } i \neq j, j \in I_n\} \tag{6}$$

Other application use what are called perpendicular bisector, or PEBI, volumes (Palagi and Aziz 1991) and
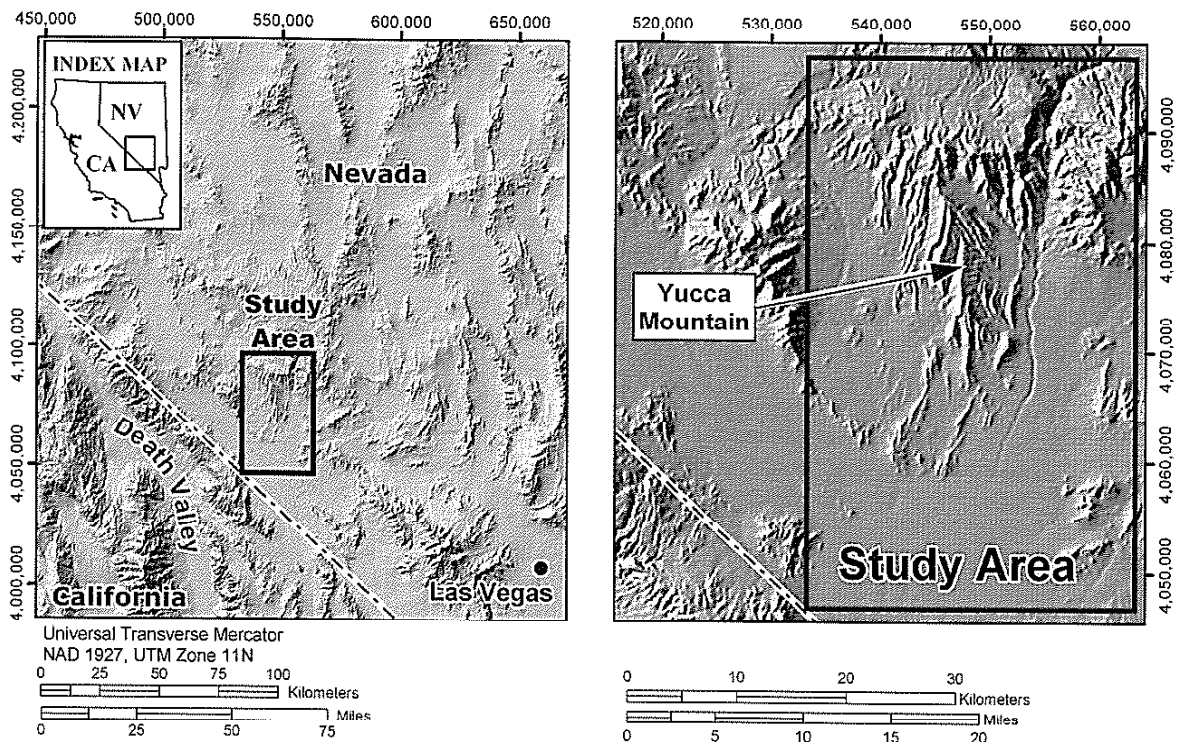
Figure 2. A map of the study area.

median mesh control volumes. The Voronoi diagram is derived in practice from the two- or three-dimensional Delaunay triangulation of the point distribution. The CVFE representation of Equation 1 is

$$V_i \frac{(A_{mass}^{t+1} - A_{mass}^t)}{\Delta t} - \sum_{j \neq i} \frac{A_{ij}}{d_{ij}} \frac{k\rho}{\mu} \left[(P_j - P_i) - \left(\frac{P_i + P_j}{2}\right) \rho g (x_{3,j} - x_{3,i}) \right]$$
$$+ q_{i,mass} = 0 \qquad i = 1,N \qquad (7)$$

where A_{ij} and d_{ij} are the area of the Voronoi boundary between two nodes and the distance between connected nodes i and j, respectively; V_i is the volume of the Voronoi cell around node i; and N is the number of nodes. The solute conservation equation (Equation 5) is discretized in a similar fashion.

The matrix coefficients (i.e., elements of the stiffness matrix) of the traditional finite element method can be interpreted as a linear function of the area through which the fluid passes traveling from one node to its neighbor. An unstructured sparse matrix of area coefficients composed of the area of the boundary of each Voronoi volume that separates adjacent nodes is the final output of the grid generation process. This matrix contains topological information about the connectivity of the grid, but does not explicitly contain information of the grid geometry.

These terms are used to form control volume difference equations for the conservation equations. This method differs from traditional finite element methods in that material properties are defined by node, not element.

In FEHM, the nodal definition of equation parameters leads naturally to a separation of the nonlinear and purely geometric parts. This separation is explained in detail in Fung et al. (1994) and is valid over lower order elements.

The nonlinear part uses an average, $D = k\rho/\mu$, between two nodes. This is usually taken to be the upstream nodal value, but other methods of handling heterogeneities are possible. The result is a much more stable method for solving nonlinear problems while still retaining much of the geometric flexibility of finite elements. The method has been used in FEHM since 1983 (Zyvoloski 1983) and has been extensively verified (Dash et al. 1995). A harmonic weighting of the permeability is used. Newton-Raphson iteration is applied to the system of equations. The system of equations is solved with a multidegree of freedom, preconditioned, conjugate gradient methods using generalized minimum residual (GMRES) (Saad and Schultz 1986), biconjugate gradient squared acceleration techniques. It should be noted that the focus of this paper is geometry and truncation errors, and that the fluid equation coefficients (e.g., permeability,
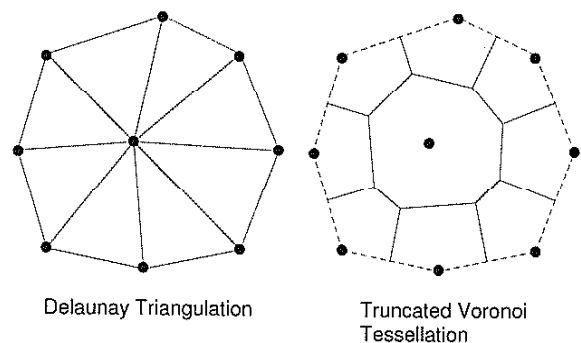

Delaunay Triangulation   Truncated Voronoi Tessellation

Figure 3. An example of a Delaunay triangulation and truncated Voronoi tesselation for the same node distribution.

porosity) for problems in this work are constant in time, but heterogeneous in space.

Interpolation of Material Properties from Hydrogeologic Framework to Computational Grid

GEOMESH (Gable et al. 1995) is an unstructured grid generator developed to represent geologic volumes in two and three dimensions. It can be used to build a grid representing geologic structure such as layers, faults, and intrusions. Nodes are connected within GEOMESH to form a Delaunay mesh from which the Voronoi coefficients are computed. The elements are triangles if the grid is two-dimensional or tetrahedra if the grid is three-dimensional. A material number, in addition to other real or integer attributes (e.g., density, permeability, porosity), is associated with each element or node. Attributes are integer or real valued properties assigned to nodes or elements. For ground water modeling, these attributes may be permeability, porosity, rock density, etc. Attribute distributions can be inspected visually using standard graphics packages that support unstructured finite element data types. GEOMESH ensures that the geometry of the input model describing the conceptual geology is preserved within the tolerance specified.

In situations where the computational grid will not be designed to conform to geometry, an alternative is to use the original hydrogeologic framework, G_{source}, as a source for interpolation of hydrogeologic properties onto the computational grid, G_{sink}. Grid to grid interpolation, from a source grid to a sink grid, allows for the virtual superposition on G_{sink} of the node or element attributes belonging to G_{source}. The best results are obtained if G_{sink} is of equal or higher resolution than the G_{source} grid. The two grids should generally be of the same volume and location, but they do not have to coincide exactly. They do not have to have the same resolution or element type. Either can be structured or unstructured. There are currently three ways to interpolate material attributes from grid G_{source} to nodes of grid G_{sink}. There are also methods, not described here, for interpolating onto elements of a sink grid.

Interpolation Algorithms

Source Node Attribute with Real Values onto Sink Node Attribute

GEOMESH locates a G_{sink} node within an element of G_{source}. The attribute of the nodes defining the element of G_{source} are then interpolated. That is, if the attribute estimate, $f(\bar{u})$, is desired at the coordinate, $\bar{u}$, given $f(\bar{x}_j)$ where $\bar{x}_j$ are the j coordinates of the element nodes, then $\bar{u}$ can be written as

$$\bar{u} = \sum_{j=1}^{nodes} \lambda_j \bar{x}_j \tag{8}$$

where

$$1 = \sum_{j=1}^{nodes} \lambda_j \tag{9}$$

and

$$0 \leq \lambda_j \leq 1 \tag{10}$$

Then the interpolation of the nodal values is

$$f(\bar{u}) = \sum_{j=1}^{nodes} \lambda_j f(\bar{x}_j) \tag{11}$$

The interpolation of the node attribute of the element in G_{source} is assigned as the attribute of the node of G_{sink}.

Source Element Attribute with Integer Values onto Sink Node Attribute

GEOMESH locates a G_{sink} node within an element of G_{source} (Figure 4). The attribute value of the G_{source} element is assigned to the G_{sink} node attribute. If the G_{sink} node falls on a boundary between two or more elements possessing different attributes, the user can specify a way to decide which value of attribute to assign to the G_{sink} node. This study uses this method for interpolating hydrostratigraphic unit attributes and specifies the use of the maximum attribute value found at any boundaries between elements of G_{source}.

Source Node Attribute with Integer Values onto Sink Node Attribute

GEOMESH uses a nearest neighbor approach by locating a G_{sink} node within a Voronoi cell of G_{source}. The attribute of the node within the Voronoi cell of G_{source} is assigned as the attribute of the node of G_{sink}. If the G_{sink} node falls on a boundary between two or more Voronoi

Grid G*source*   **Grid G*sink* Nodes**

Superposition of Grid G*sink* Nodes on Grid G*source*   **Grid G*sink* Node Attributes Interpolated from Grid G*source***
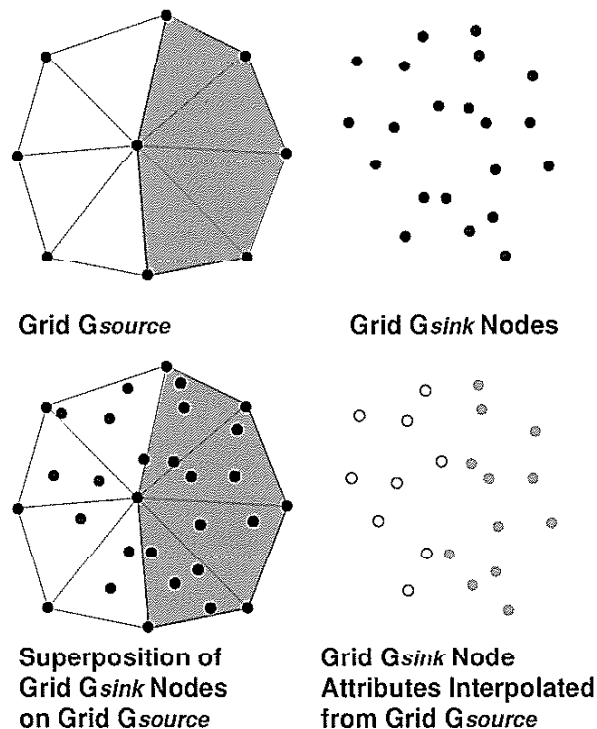
Figure 4. Schematic outline of a method to interpolate integer element attribute values of G_{source} onto nodes of G_{sink}. Each node of G_{sink} is identified with an element of G_{source} and the material property of each element is assigned to the node-based material properties used in calculations.

Table 1
Hydrostratigraphic Units, Permeabilities and Volumes

Material Number	Name	Material Volume (m³)	Permeability (m²)
4	Granitic confining unit	0.2387375E+10	3.5e-14
5	Lower carbonate aquifer	0.4969478E+10	3.3e-12
6	Lower clastic confining unit	0.2285245E+12	2.0e-15
7	Lower carbonate aquifer	0.3930128E+12	3.3e-12
8	Upper clastic confining unit	0.3113249E+12	5.5e-19
9	Lower carbonate aquifer	0.1231588E+09	3.3e-12
10	Upper carbonate aquifer	0.7581275E+09	6.7e-13
11	Undifferentiated valley-fill	0.1699669E+12	2.9e-14
12	Lower volcanic confining unit	0.1021979E+12	1.0e-16
13	Lower volcanic aquifer	0.7413871E+11	5.0e-13
14	Middle volcanic confining unit	0.2513773E+12	1.9e-16
15	Middle volcanic aquifer	0.2169467E+12	6.0e-15
16	Upper volcanic confining unit	0.4169756E+11	1.0e-18
17	Upper volcanic aquifer	0.5746906E+11	6.0e-15
18	Lava-flow aquifer	0.7076574E+10	4.5e-14
19	Lacrustine aquifer	0.4196269E+09	1.0e-14
20	Valley-fill confining unit	0.1209244E+09	3.0e-16
21	Valley-fill aquifer	0.1189373E+11	6.6e-14
1, 2 ,3, 22, 23	Outside geologic geometry framework		1.0e-32 (1.0e-12 for top to bottom flow runs)

cells, the user can specify whether to use the maximum or minimum attribute value.

Each of these methods is straightforward; however, the implementation must be done in a way that allows application to large problems, (e.g., sink and source $O[10^6]$). The majority of the computational work is in searching for the node or element in the grid G_{source} that is near a particular node of the G_{sink}. The implementation in GEOMESH uses a KD-tree algorithm to accelerate the search process. This is a standard algorithm for building a binary tree for searching multidimensional point distributions (deBerg et al. 2000). Without this, it would be impractical to perform grid-to-grid interpolation in cases where the source and sink grids are large.

Thus, the spatial distribution of material properties from a hydrostratigraphic model, G_{source}, is interpolated onto a structured grid, G_{sink}. The structured orthogonal grids used in this study are better able to capture the conceptual geometry if they are of finer resolution.

Problem Description

The saturated zone of the Yucca Mountain site was chosen to test for the ability of the structured orthogonal grids to capture the hydrostratigraphy of the hydrogeologic framework model (Figure 1). The area of interest is contained within Nevada State Coordinates of 533,340 to 563,340 m in an east-west direction, 4,046,782 to 4,091,782 m in the north-south direction, and −755 to 1196 m vertically above sea level (Figure 2). This area contains the ground water flow system of interest. The water table lies ~400 m below the proposed high level nuclear

waste repository. Any radionuclides that might be released would have to migrate downward through the unsaturated zone to reach the saturated zone.

Eighteen distinct hydrostratigraphic materials are located within this volume as shown in Figure 1 and listed in Table 1. Materials 1, 2, 3, 22, and 23 have been added to create a buffer zone that allows a rectangular model to be used. The geologic material consists of Paleozoic carbonate rock aquifers and siliceous clastic confining beds with some Miocene volcanic rocks present. The ground water flow is highly compartmentalized due to structural and lithologic features. Ground water flow is generally from north to south due to a decrease in average topographic elevations (Rousseau et al. 1996).

The discretization of the conceptual geologic framework is at a 250 m horizontal spacing. Permeabilities are determined by inverse modeling performed by Czarnecki et al. (1997) on a previous geologic framework discretized at 1500 m. The permeability and volume of the materials are listed in Table 1.

Actual ground water flow at this site is predominately from north to south. However, to demonstrate the importance of the geology to the choice of grid resolution, at each grid resolution used, three different fluid flows are computed, each using a different boundary condition. The boundary conditions chosen do not reflect the actual head gradients at Yucca Mountain. They are arbitrary values chosen to test grid resolution, but are not representative of the actual system. The first boundary condition used is a fixed head difference of 1531 m on the north and south boundaries. The second boundary condition used is a fixed head difference of 1531 m on the east and west boundaries. The third boundary condition used is a fixed head difference of 1531 m on the top and bottom boundaries. The goal is not to reproduce the actual flow system that exists at the site, but to test the sensitivity of the flow and transport in three orthogonal directions to changes in the mesh resolution. The vertical flow components generated between the top and bottom fixed head difference boundaries are important despite regional flow being predominately north to south because the heterogeneity of the geology would likely contribute to generation of vertical flowpaths. Although a calibrated model must have appropriate head at each inlet and outflow boundary, the actual head differential between boundaries is not important to a grid resolution study. This is equivalent to three different models for each grid resolution with three resulting hydraulic gradients between parallel boundaries of 0.034 from north to south, 0.051 from east to west, and 0.78 from top to bottom. Steady state, constant density, isothermal saturated flow with specified head difference on two opposite boundaries, and no flow boundaries on the other four sides is solved using FEHM. The total flow out of the model is compared for each grid.

Solute transport is modeled using the calculated steady state flow solutions from half of the grids (Table 2 grid numbers 1, 3, 5, 7, and 9). Only the north-south flow field condition is used for the solute transport modeling. The north boundary of the grid is fixed at a constant solute flux of 70 mol/s. This solute flux results in an average boundary concentration of ~1 mol/kg. Since the aquifer is inhomogeneous,

Table 2
Details of Grid Resolution

Grid Number	Total Number of Nodes	Number of Nodes x and y Direction	Number of Nodes y Direction	Node Space x Direction (m)	Node Space y Direction (m)	Nodes Space z Direction (m)
1	96	4	6	10,000	9000	650
2	175	5	7	7500	7500	488
3	1053	9	13	3750	3750	244
4	7225	17	25	1875	1875	122
5	23,125	25	37	1250	1250	81
6	40,500	30	45	1034	1023	67
7	63,700	35	52	882	882	57
8	96,000	40	60	769	763	50
9	165,888	48	72	638	633	42
10	324,000	60	90	508	506	33

the fluid flux varies over the north boundary and produces variable solute concentrations at the boundary. All solute transport models are run to a total time of 10^6 yr to allow the solute to reach the south boundary. The solute is non-absorbing, nondecaying, and nonreactive. The dispersivities used are homogeneous with values of 50 and 5 m, respectively, for the longitudinal and transverse directions.
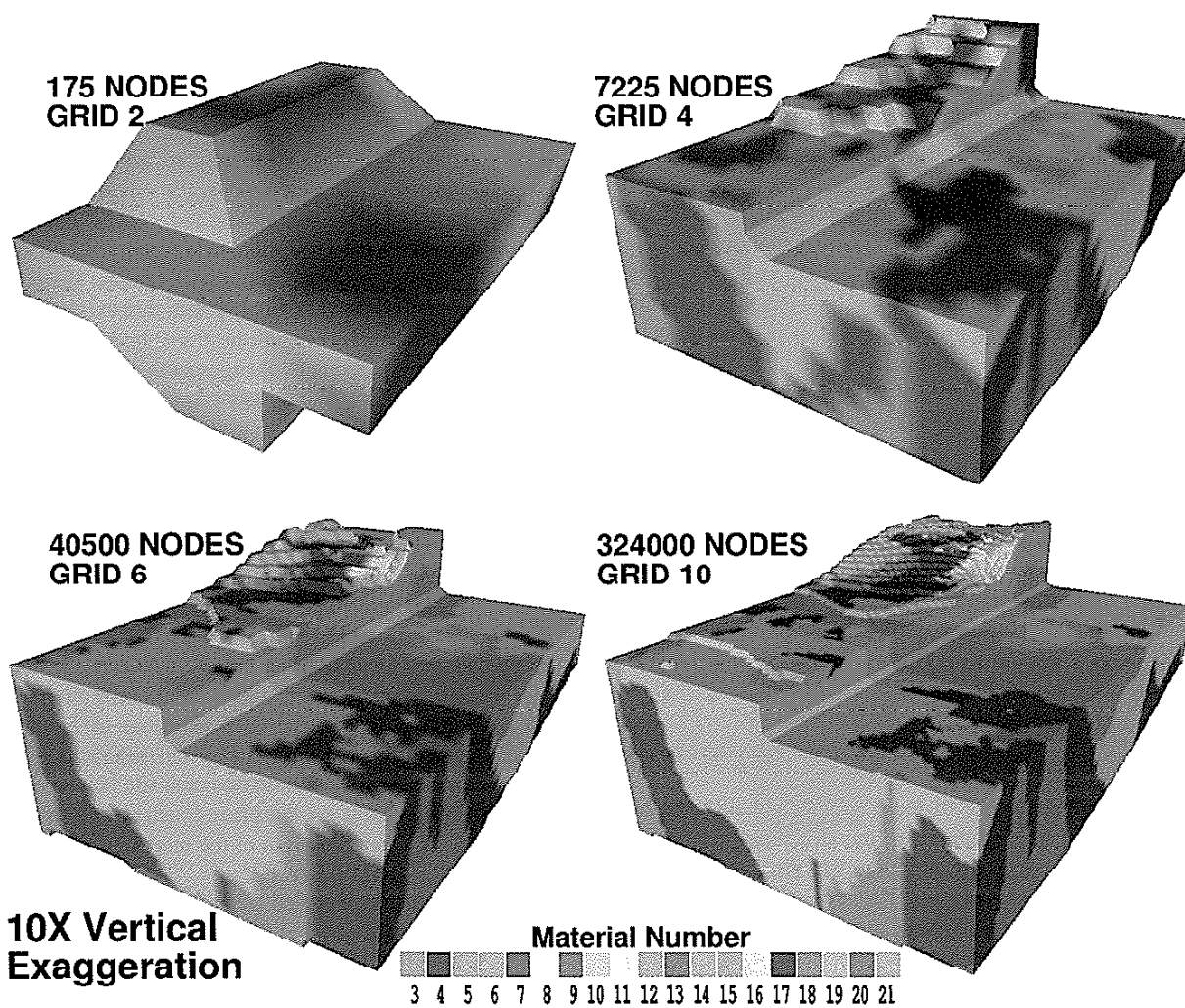

Figure 5. Structured grid material distribution at four different resolutions (10× vertical exaggeration). A block of material from the upper right side is cut away to expose the interior. Buffer zones on the top and bottom are not shown. Table 1 relates material number to geological unit names.

The fluid flow problem is designed to study the sensitivity and variability of results introduced by the grid resolution used to represent hydrostratigraphy. In order to test numerical errors due to truncation errors associated with grid spacing, a single material property of constant permeability could be used. However, this flow solution is a linear variation in head with a corresponding constant flux. Tests with homogeneous properties on orthogonal grids confirm this result. The differences in reported fluid fluxes using inhomogeneous grids are a result only of representation errors of the hydrogeologic units. The outlet fluid flux was chosen as the parameter for comparison of fluid flow models because this is a major factor influencing potential radionuclide transport to the accessible environment.

The outlet solute flux is chosen as the diagnostic quantity for comparison of solute transport calculations on different grids. Grid resolution may have a numerical effect on the solute transport results due to numerical dispersion. This effect usually would add to the effect of the heterogeneous materials. Homogenous versions of grids 1, 3, and 8 are used to determine the effect of numerical dispersion on the solute transport results. The outlet solute fluxes for homogeneous grids 1, 3, and 8 at 10^6 yr are all $< 1 \times 10^{-6}$ mol/s. This is approximately 10^{-5}% of the outlet solute flux results for the heterogeneous cases at all the grid resolutions because the heterogeneous materials create fast flowpaths. Any effect of numerical dispersion due to changes in grid resolution is thus judged to be insignificant in this study.

Results

Ten structured grids are constructed using GEOMESH and hydrologic properties are interpolated onto them from the tetrahedral hydrostratigraphic framework. The number of nodes in each of the x, y, and z directions are chosen so that the nodes in any x-y plane have spacing with $\Delta x \cong \Delta y$ = *constant* and the number of nodes in the z direction are equal to the number in the x direction. The nodes are connected into tetrahedral elements. The grid details are given in Table 2. For visual comparison with the stratigraphic model, the material distribution for grids 2, 4, 6, and 10 are shown in Figure 5.

The interpolation algorithms work by determining the material number of the element of the hydrostratigraphic model grid, G_{source}, that the structured computational grid node, G_{sink}, is located within. Any nodes from the structured grid that fall outside the hydrostratigraphic model grid geometry are assigned a special material type defined as a buffer zone. The buffer zone material type is assigned a very low permeability and has insignificant effects on the modeling results. Since the nodal locations are different for each of the 10 grids constructed, the volumes of each material changes from grid to grid.

Consider grid 2 (Figure 5) which has 5 by 7 nodes horizontally and 5 vertical nodes. The interpolated representation of the hydrostratigraphic model from G_{source} to G_{sink} is inaccurate as the material distribution in G_{source} is more detailed than the nodal distribution in grid 2 will allow. Thus, the details of the material distribution are missing in grid 2 and the buffer zones at the top and bottom of grid 2

are not well defined (though not explicitly shown in Figure 5). Compare the material distribution of grid 2 to that of grid 6 in Figure 5. Grid 6 has 30 by 45 nodes horizontally and 30 nodes vertically. Grid 6 captures the material distributions in G_{source} much more accurately than grid 2, and the buffer zones at the top and bottom of the grid are very well defined. Thus, grid 6 better represents the hydrostratigraphy. However, even with the high-resolution grid of grid 10, every material geometry may not be captured accurately. Any node of a G_{sink} in a high-resolution grid may fall just outside the boundary of an important material type in G_{source}, thus missing capturing that material boundary accurately in the computational grid.

The normalized volume of each material type captured by each grid is shown in Figure 6. The percentage of the total volume of each material in the hydrostratigraphic framework model is shown in Figure 7. The finer the structured grid, the more closely the volumes of the materials match those of the stratigraphic model. It is evident from Figures 6 and 7 that materials with large volumes converge to their true value more rapidly and are less affected by low resolution grids than stratigraphic units with small volume.

Each of the 10 grids is used to model confined flow through the saturated zone. A head difference of 1531 m is applied on alternate parallel pairs of boundaries. Figure 8 shows ground water head contours for grids 2, 4, 6, and 8 for north to south flow. Note that a high head gradient results for grids 6 and 8, but not for grids 2 or 4. This difference in the head distribution is solely due to greater accuracy by higher resolution grids in capturing the hydrostratigraphy. The high head gradient for high-resolution grids also results from models of east to west flow and are probably caused by the very low permeabilities of materials 8 and 16. When more realistic modeling of the boundary conditions is performed, these high gradients do not result.

The resulting fluid flux out at the lower fixed head boundary of the model is used to compare the effectiveness
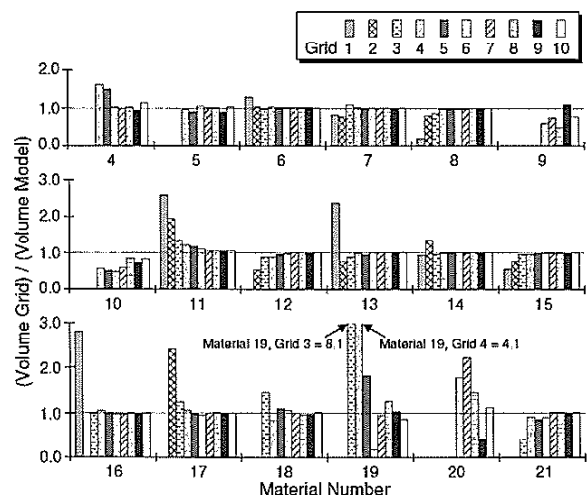

Figure 6. Ratio of structured grid material volume for each grid resolution to conceptual grid material volume.
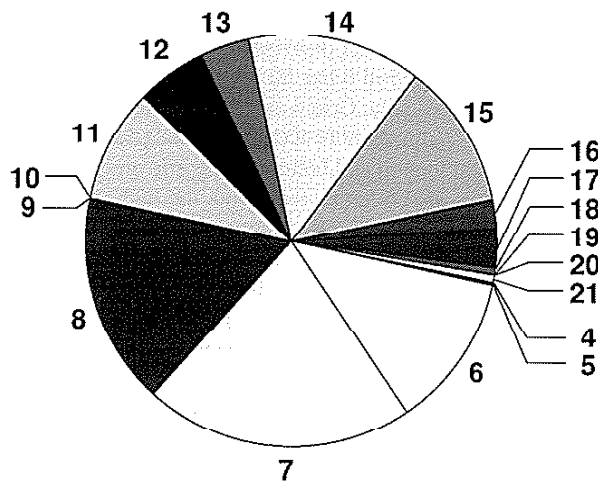
Figure 7. Volume of each material type within total computational grid volume. Materials 1, 2, 3, 22, and 23, which are buffer volumes, have not been included.

of each grid in representing the hydrostratigraphy on flow behavior. The resulting fluid flux from each grid is shown in Figure 9. The curve shows asymptotic behavior with increased resolution. The difference in flow between grids 9 and 10 for the north to south boundary condition is 2%. The difference in flow between grids 9 and 10 for the east to west boundary condition is 5%. The difference in flow between grids 9 and 10 for the top to bottom boundary condition is 3%. Since higher grid resolution is more expensive, this information can be used to determine at what resolution the desired accuracy would be attained.

Calculation of fluid flux changes with grid resolution can be more easily understood in terms of average grid spacing. The range of grid spacings in the vertical direction range from 650 to 33 m. Figure 9 suggests that fluid flow computations for the top to bottom fluid flow boundary conditions approach asymptotic conditions somewhere between the resolutions of grids 4 and 5. This suggests that a vertical grid spacing of 100 m and a horizontal grid spacing of 1550 m may be sufficient to model fluid flow between the top and bottom of this geology if a structured orthogonal grid is used. Similar acceptable grid resolutions may be determined using asymptotic conditions in Figure 9 for east to west flow and north to south flow.

The results of the hypothetical solute transport flux out of the south boundary of the model are shown in Figure 10
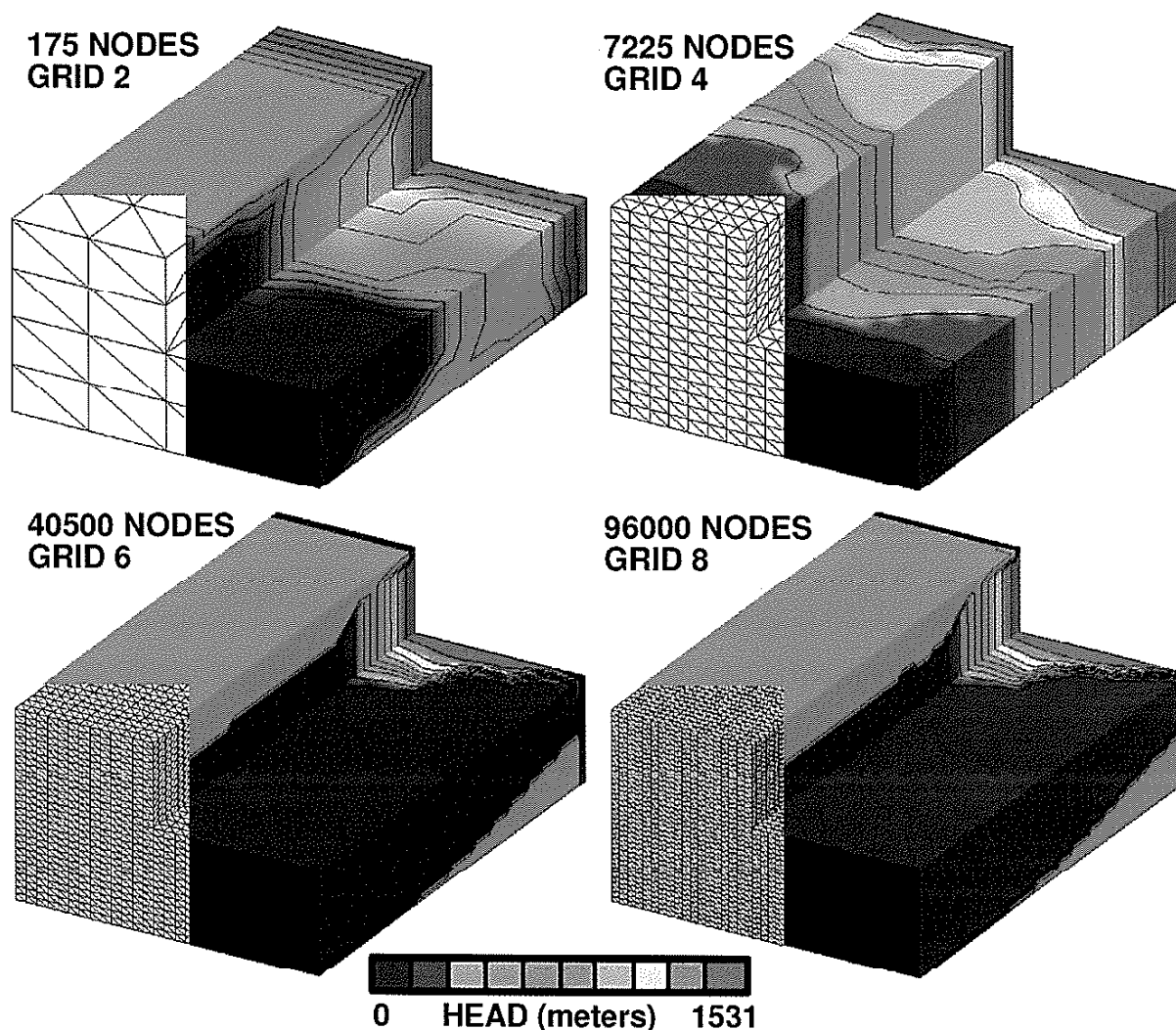

Figure 8. Head contours for calculation with north to south head gradient on four different resolution grids (10 × vertical exaggeration). A block of material from the upper right side is cut away to expose the interior. Buffer zones are not shown.
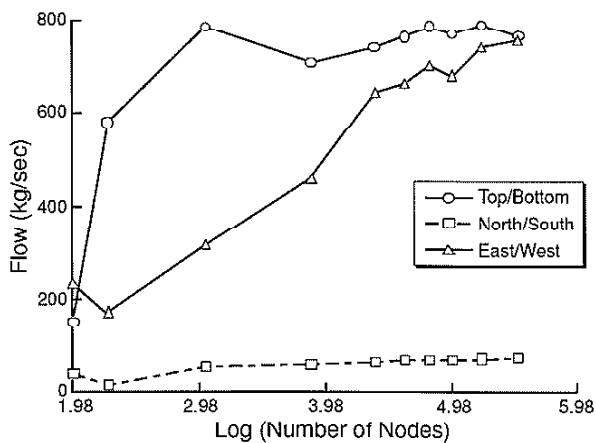
Figure 9. Fluid flow across model boundary as a function of grid resolution for all three head difference boundary conditions.

for grids 1, 3, 5, 7, and 9. Because the fluid flow field at steady state is different for each grid, a different amount of fluid has transported the solute during any fixed time period in each of the grids. Therefore, the solute flux is plotted as a function of total fluid volume instead of time in Figure 10. As the grid resolution increases, the calculations show convergent behavior. Comparing solute flux for grids 7 and 9 at fluid volume of 2×10^7 m^3, the difference in solute flux is 2%. This indicates that the resolution of grid 7 is probably adequate for solute transport modeling. Again, the resolution of the grid chosen for more accurate modeling studies is dependent on the desired accuracy of solution.

Conclusions

The grid resolution used to resolve a particular problem depends on many factors. These include geometric complexity, variability in material properties, the physics of the problem being solved, and boundary conditions, as well as economic factors and potential risk. The case study presented demonstrates examples of diagnostic quantities (total fluid flux, solute mass flux) that can be used to quantitatively measure the sensitivity of results to grid resolution.
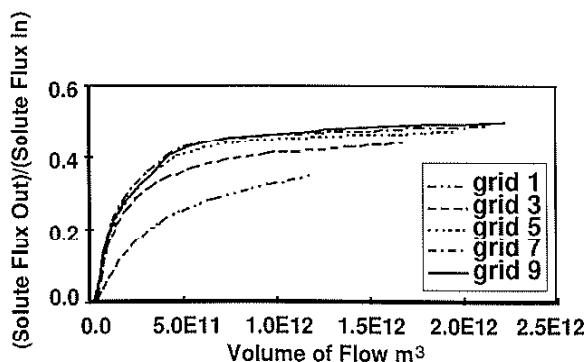

Figure 10. Fraction of solute flux leaving south end of grid as a function of the volume of fluid flow that has moved through the reservoir.

In this case study, the geologic and hydrostratigraphy properties of the ground water zone in the vicinity of Yucca Mountain are used to create a conceptual model for modeling hypothetical ground water flow and solute transport. Orthogonal structured grids of 10 different resolutions are created from the hydrogeologic framework model to reflect the hydrogeology for flow and solute transport numerical models. The grids are used to perform CVFE modeling of the ground water flow and solute transport. The outflow at steady state is used to compare the ability of the grids to capture the effect of the hydrostratigraphy.

As the resolution of the grids increases and the material distribution is better represented by the grid, the computed fluid flow changes, but begins to exhibit asymptotic behavior. One can use this method to choose which grid resolution will best model the flow with the accuracy desired.

As the resolution of the grids increases, the solute flux at the model outlet boundary changes. However, with increasing resolution, the solute flux exhibits convergent behavior. Again, one can use this method to chose the resolution that will best model the solute transport with the result accuracy desired.

Based on the convergence behavior observed in a set of 10 progressively finer grids, it is estimated that horizontal grid spacing of O (500 m) and vertical grid spacing of O (40 m) resolve the fluid flux to within 5% of the value that would be obtained if flow and transport analysis were performed on even finer grids. For calculation of solute transport, the same resolution is estimated to resolve the solute flux to within 5%.

Acknowledgments

References

Civilian Radioactive Waste Management System Management and Operating Contractor. 2000. Calibration of the site-scale saturated zone flow model. MDL-NBSHS–000011 REV 00.

Czarnecki, J.B., C.C. Faunt, C.W. Gable, and G.A. Zyvoloski. 1997. Preliminary three-dimensional finite-element groundwater flow model of the saturated zone, Yucca Mountain, Nevada. U.S. Geological Survey YMP Milestone Number SP23NM3.

D'Agnese, F.A., C.C. Faunt, A.K. Turner, and M.C. Hill. 1997. Hydrogeologic evaluation and numerical simulation of the Death Valley regional ground-water flow system, Nevada and California. U.S. Geological Survey Water-Resources Investigations Report 96–4300.

Dash, Z.V., B.A. Robinson, and G.A. Zyvoloski. 1995. V&V report for the FEHMN application. Los Alamos National Laboratory Report LA-UR–95–2063.

DeBerg, M., M. van Kreveld, M. Overmars, and O. Schwarzkopf. 2000. *Computational Geometry Algorithms and Applications*. Berlin: Springer-Verlag.

Eddebbarh, A.A., G.A. Zyvoloski, B.A. Robinson, E.M. Kwicklis, P.W. Reimus, B.W. Arnold, T. Corbet, S.P. Kuzio, and C. Faunt. 2003. The saturated zone at Yucca Mountain: An overview of the characterization and assessment of the saturated zone as a barrier to potential radionuclide migration. *Journal of Contaminant Hydrology* 62, no. 3: 477–493.

Feehley, C.E., C. Zheng, and F.J. Molz. 2000. A dual-domain mass transfer approach for modeling solute transport in heterogeneous aquifers: Application to the macrodispersion experiment (MADE) site. *Water Resources Research* 36, no. 9: 2501–2515.

Frind, E.O., E.A. Sudicky, and S.L. Schellenberg. 1988. Microscale modelling in the study of plume evolution in heterogeneous media. In *Groundwater Flow and Quality Modelling*, ed. E. Custodio, A. Gurgui, and J.P. Lobo Ferreira. D. Dordrecht, Netherlands: Reidel Publishing Co.

Forsyth, P.A. 1989. A control volume finite element method for local mesh refinement. In *SPE 18415, the SPE Symposium on Reservoir Simulation*, February 6–8, Houston, Texas. Houston, Texas: Society of Petroleum Engineers.

Forsyth, P.A. 1991. A control volume finite-element approach to NAPL groundwater contamination. *SIAM Journal on Scientific Computing* 12, no. 5: 1029–1057.

Fung, L.S., L. Buchanan, and R. Sharma. 1994. Hybrid CVFE method for flexible-grid reservoir simulation. *SPE Journal* 19, 188–199.

Gable, C.W., H.E. Trease, and T.A. Cherry. 1996. Geological applications of automatic grid generation tools for finite elements applied to porous flow modeling. In *Numerical Grid Generation in Computation Fluid Dynamics and Related Fields*, ed. B.K. Soni, J.F. Thompson, H. Hausser, and P.R. Eiseman. Starkville, Mississippi: Mississippi State University Press.

Gable, C.W., T.A. Cherry, H.E. Trease, and G.A. Zyvoloski. 1995. GEOMESH grid generation. Los Alamos National Laboratory Report LA-UR–95–4143.

George, D.C. 2000. LaGriT user's manual. http://www.t12.lanl.gov/~lagrit).

Haitjema, H., V. Kelson, and W. de Lang. 2001. Selecting MODFLOW cell size for accurate flow fields. *Ground Water* 39, no. 6: 931–938.

Heinemann, Z.E., and C.W. Brand. 1988. Gridding techniques in reservoir simulation. In *Proceedings of the First International Forum on Reservoir Simulation*, September 12–16, Alpach, Austria, 339–425.

Luckey, R.R., P. Tucci, C.C. Faunt, E.M. Ervin, W.C. Steinkampf, F.A. D'Agnese, and G.L. Patterson. 1996. Status of understanding of the saturated-zone ground-water flow system at Yucca Mountain, Nevada, as of 1995. U.S. Geological Survey Water-Resources Investigations Report 96-4077.

Okabe, A., B. Boots, and K. Sugihara. 1992. *Spatial Tessellations: Concepts and Applications of Voronoi Diagrams*. New York: Wiley & Sons.

Palagi, C., and K. Aziz. 1991. Use of Voronoi grids in reservoir simulation. In *SPE 11889 and 26951, Proceedings of the SPE 66th Annual Technical Conference and Exhibition*, October 6–9, Dallas, Texas. Houston, Texas: Society of Petroleum Engineers.

Robinson, B.A., H.S. Viswanathan, A.V. Wolfsberg, C.W. Gable, and G. Bussod. 1997. The site-scale unsaturated zone transport model of Yucca Mountain. Los Alamos National Laboratory YMP Milestone SP25BMC.

Rousseau, J.P., E.M. Kwicklis, and D.C. Gillies (ed.). 1996. Hydrogeology of the unsaturated zone, north ramp area of the exploratory studies facility, Yucca Mountain, Nevada. U.S. Geological Survey Water-Resources Investigations Report 96–4050.

Saad, Y., and M. Schulttz. 1986. GMRES: A generalized minimal residual algorithm for solving nonsymmetric linear systems. *SIAM Journal of Scientific Computing* 7, 856–869.

Trease, H., D.C. George, C.W. Gable, J. Fowler, A. Kuprat, and A. Khamyaseh. 1996. The X3D grid generation system. *Numerical Grid Generation in Computational Fluid Dynamics and Related Fields*, ed. B.K. Soni, J.F. Thompson, H. Hausser and P.R. Eiseman. Starkville, Mississippi: Mississippi State University Press.

Verma, S.K. 1996. Flexible grids for reservoir simulation. Ph.D. thesis, Stanford University, California.

Viswanathan, H.S., B.A. Robinson, A.J. Volocchi, and I.A.Triay. 1998. A reactive transport model of neptunium migration from the potential repository at Yucca Mountain. *Journal of Hydrology* 209, 251–280.

Voronoi, G. 1908. Nouvelles applications des parametres continus a la theorie des formes quadratiques. *Journal für die reine und angewandte Mathematik* 134, 198–287.

Ward, D.S., D.R. Buss, J.W. Mercer, and S.S. Hughes. 1987. Evaluation of a groundwater corrective action at the Chem-Dyne hazardous waste site using a telescopic mesh refinement modeling approach. *Water Resources Research* 23, no. 4: 603–617.

Zyvoloski, G. 1983. Finite element methods for geothermal reservoir simulation. *International Journal for Numerical and Analytical Methods in Geomechanics* 7, 75–86.

Zyvoloski, G., Z. Dash, and S. Kelkar. 1991. FEHMN 1.0: Finite element heat and mass transfer code. Los Alamos National Laboratory Report LA–12062-MS.

Zyvoloski, G., E. Kwicklis, A. Eddebbarh, B. Arnold, C. Faunt, and B.A. Robinson. 2003. The site-scale saturated-zone flow model for Yucca Mountain: Calibration of different conceptual models and their impact on flow paths. *Journal of Contaminant Hydrology*, 62, no. 3: 731–750.